J. Fluid Mech. (2009), *vol.* 640, *pp.* 441–452.
doi:10.1017/S0022112009991480

Effect of dispersion on the onset of convection during CO_2 sequestration

JUAN J. HIDALGO[1,2]† AND JESÚS CARRERA[2]

[1]Department of Geotechnical Engineering and Geosciences, School of Civil Engineering, Technical University of Catalonia (UPC), C. Jordi Girona 1-3, 08034 Barcelona, Spain

[2]Institute of Environmental Assessment and Water Research, Spanish National Research Council (IDAEA-CSIC), C. Jordi Girona 18, 08034 Barcelona, Spain

(Received 5 May 2009; revised 1 August 2009; accepted 3 August 2009; first published online 19 October 2009)

Dissolution of carbon dioxide (CO_2) injected into saline aquifers causes an unstable high-density diffusive front. Understanding how instability fingers develop has received much attention because they accelerate dissolution trapping, which favours long-term sequestration. The time for the onset of convection as the dominant transport mechanism has been traditionally studied by neglecting dispersion and treating the CO_2–brine interface as a prescribed concentration boundary by analogy to a thermal convection problem. This work explores the effect of these simplifications. Results show that accounting for the CO_2 mass flux across the prescribed concentration boundary has little effect on the onset of convection. However, accounting for dispersion causes a reduction of up to two orders of magnitude on the onset time. This implies that CO_2 dissolution can be accelerated by activating dispersion as a transport mechanism, which can be achieved adopting a fluctuating injection regime.

1. Introduction

Carbon dioxide (CO_2) injection in saline aquifers has been proposed as a method to reduce greenhouse gas emissions (IPCC 2005). CO_2 is injected under a cap rock forming a plume less dense than the brine, which floats while spreading horizontally. CO_2 dissolves in the underlying brine, which is favourable for several reasons. First, it facilitates the transformation of CO_2 to more stable species such as bicarbonate or, if geological conditions are propitious, solid mineral carbonates (Lackner *et al.* 1995). Second, it reduces the risk of upward leaks both because the viscosity of brine is much larger than that of any CO_2 phase (Adams & Bachu 2002) and because CO_2-rich brine is 1–2 % denser than resident brine (Yang & Gu 2006). The resulting conditions (denser liquid on top) are unstable so that CO_2-rich brine will tend to sink.

CO_2 dissolution into the brine is initially controlled by diffusion, which is a slow process with mass flux evolving as $t^{-1/2}$, where t is time. As time passes, the small perturbations of the CO_2 diffusive front caused by heterogeneity or a fluctuating injection regime will tend to strengthen. That is, when enough CO_2 has dissolved, the perturbations will tend to progress, causing CO_2-rich brine to sink as fingers into the CO_2-free brine, which is termed the convective regime. The onset of this regime is important because by bringing dissolved CO_2 away from the dissolution front, CO_2

† Email address for correspondence: juan.hidalgo@upc.edu

dissolution is enhanced (Lindeberg & Bergmo 2003), which favours the sequestration process. However, it can take a long time to develop.

The conditions under which convection is activated have received great attention in recent years. Conceptually, CO_2 dissolution is an unstable boundary-layer problem analogous to the one found when a fluid is overlaid by a cold boundary (Rees, Selim & Ennis-King 2008). Following this analogy, CO_2 dissolution is solved in a semi-infinite domain with a top impervious boundary where concentration is prescribed equal to CO_2 solubility. The brine is assumed incompressible, the Boussinesq approximation valid and the porous medium homogeneous. Under these assumptions, the time for the onset of convection is inversely proportional to the square of permeability (Lindeberg & Bergmo 2003). In fact, the onset time decreases when either horizontal or vertical permeabilities increase (Xu, Chen & Zhang 2006). Linear stability analysis can be performed on the basis of a Rayleigh number computed using the domain thickness (Hassanzadeh, Pooladi-Darvish & Keith 2005; Riaz *et al.* 2006). Yet, results show that the time for the onset of convection is not dependent on the Rayleigh number (Riaz *et al.* 2006). This is reasonable because convection only affects the aquifer top and should not be sensitive to the thickness of the aquifer. Therefore, it should not depend on the Rayleigh number (Riaz *et al.* 2006; Rees *et al.* 2008).

Several issues concerning this conceptual model can be raised that may affect the time for the onset of convection. The first one is the analogy to a heat transport problem. In a heat transport model, the fluid may be assumed to consist of a single component. Heat transport and fluid flow are basically linked through the buoyancy term. However, in mass transport problems the fluid must be viewed as consisting of at least two components (i.e. brine and CO_2). Since the flow equation expresses the mass balance of the whole fluid phase, additions of any of the two components must be accounted for in the mass balance. Specifically, while an impervious boundary (i.e. a boundary with zero brine flux) can be treated as a zero mass flux in thermal problems, it must allow for fluid mass flux (CO_2 component) in mass transport problems (Hassanizadeh & Leijnse 1988; Hidalgo, Carrera & Medina 2009*b*).

The second issue refers to the simplifications assumed for flow and transport problems. For flow, the fluid is considered incompressible and the Boussinesq approximation valid. However, fluid density increases slightly with pressure. More importantly, porosity also increases because the porous medium is also compressible, and an increment in fluid pressure will cause a decrease in effective stress (stress transmitted by the solid). As a result, fluid flux cannot be assumed divergence free. In fact, acknowledging compressibility helps in simulating the pressure rise caused by the influx of CO_2, which helps in promoting CO_2 flux downwards. The Boussinesq approximation may affect the transient solution (Johannsen 2003), although it is valid for the range of values of the Rayleigh number that will be presented here (Landman & Schotting 2007). For transport, dispersion is neglected. Hydrodynamic dispersion accounts for the effects of the deviations from the mean flow caused by heterogeneity in permeability. Heterogeneity is present in all natural systems. Therefore, dispersion has to be included in any realistic transport formulation, as pointed by Riaz *et al.* (2006). Notice that dispersion is often neglected in thermal analogies, which are the basis of many CO_2 dissolution models. This is controversial (see Ferguson & Woodbury 2005; Hidalgo, Carrera & Dentz 2009*a*) but may be justified because of the relatively large value of thermal conductivity. However, dispersion cannot be disregarded in solute transport because it is usually much larger than molecular diffusion. In fact, dispersion can be artificially increased if a fluctuating injection regime is adopted (Dentz & Carrera 2003).

The third issue relates to the choice of dimensionless numbers. The fact that the time for the onset of convection should not depend on the Rayleigh number suggests eliminating it as dimensionless number. Instead, it can be used to define the characteristic (vertical) length scale, as suggested by Rees *et al.* (2008).

The objective of this work is to address these three issues and, specifically, to assess how a more realistic representation of CO_2 dissolution affects the time for the onset of convection.

2. Governing equations

2.1. *Dimensional form*

The compressible density-dependent flow and advective–diffusive–dispersive transport equations, which govern CO_2 dissolution in a saline aquifer, are written as (e.g. Bear 1972)

$$\rho S_p \frac{\partial p}{\partial t} + \rho\theta\beta_\omega \frac{\partial \omega}{\partial t} = -\nabla\cdot(\rho \boldsymbol{u}), \tag{2.1}$$

$$\rho\theta \frac{\partial \omega}{\partial t} = -\rho \boldsymbol{u}\cdot\nabla\omega + \nabla\cdot(\rho(\theta D_m \boldsymbol{I} + \boldsymbol{D})\nabla\omega), \tag{2.2}$$

where $\rho[ML^{-3}]$ is fluid density; $S_p[M^{-1}LT^2]$ is the specific storativity; $p[ML^{-1}T^{-2}]$ is pressure; $t[T]$ is time; $\theta[-]$ is the volumetric fluid content (porosity); $\beta_\omega = (1/\rho)\,\partial\rho/\partial\omega[-]$ is considered constant; $\omega[-]$ is CO_2 mass fraction; $\boldsymbol{u}[LT^{-1}]$ is the Darcy velocity; $D_m[L^2T^{-1}]$ is the molecular diffusion coefficient; $\boldsymbol{I}$ is the identity matrix; and $\boldsymbol{D}[L^2T^{-1}]$ is the hydrodynamic dispersion tensor, given by

$$D_{ij} = \alpha_T \|\boldsymbol{u}\|\,\delta_{ij} + (\alpha_L - \alpha_T)\frac{u_i u_j}{\|\boldsymbol{u}\|} \quad (i, j = x, z), \tag{2.3}$$

where $\alpha_L[L]$ and $\alpha_T[L]$ are the longitudinal and transverse dispersivities respectively, δ_{ij} is the Kronecker delta and $\|\cdot\|$ is the Euclidean norm. Finally, the Darcy velocity $\boldsymbol{u}$ is written as

$$\boldsymbol{u} = -\frac{k}{\mu}\left(\nabla p + \rho g \hat{\boldsymbol{e}}_z\right), \tag{2.4}$$

with $k[L^2]$ the permeability, $\mu[ML^{-1}T^{-1}]$ the viscosity, $g[LT^{-2}]$ the gravity acceleration and $\hat{\boldsymbol{e}}_z$ the unit vector pointing upwards.

The domain is conceptually considered semi-infinite; i.e. there is no interaction with the lower and lateral boundaries. The dissolution interphase between the CO_2, and the brine is located at the top of the domain, i.e. $z = 0$. The brine component cannot flow across this interphase, but the mass fraction of CO_2 in the brine is prescribed at its solubility, which causes an inward flux of CO_2. Therefore, boundary conditions are written as

$$\left.\begin{aligned} -\rho\boldsymbol{u}|_b\cdot\boldsymbol{n} &= m_s \text{ if } z = 0, \\ \boldsymbol{u}|_b\cdot\boldsymbol{n} &= 0 \text{ for } x \to \pm\infty, \text{ or } z \to -\infty, \end{aligned}\right\} \tag{2.5}$$

for flow and

$$\left.\begin{aligned} \omega|_b &= \omega_s \quad \text{if } z = 0, \\ (-\boldsymbol{u}\omega + (\theta D_m \boldsymbol{I} + \boldsymbol{D})\nabla\omega)|_b\cdot\boldsymbol{n} &= 0 \quad \text{for } x \to \pm\infty, \text{ or } z \to -\infty, \end{aligned}\right\} \tag{2.6}$$

for transport. In these equations $\boldsymbol{n}$ is the unit vector normal to the boundary pointing outwards; $m_s[ML^{-2}T^{-1}]$ is the CO_2 mass flux across the top boundary; ω_s is CO_2 solubility in brine; and $|_b$ indicates evaluation at the boundary.

The conceptual model proposed by (2.1)–(2.6) introduces several modifications with respect to previous CO_2 dissolution models. First, governing equations acknowledge fluid and, especially, porous medium compressibility through the specific storativity coefficient, which accounts for water compressibility and the elastic properties of the porous matrix. Second, hydrodynamic dispersion is included as a transport mechanism. Third, density gradients are fully accounted for (i.e. the Boussinesq simplification is not assumed). Finally, boundary conditions include the CO_2 mass flux across the top boundary. This CO_2 flux is

$$m_s = (-\rho \boldsymbol{u}\omega + \rho(\theta D_m \boldsymbol{I} + \boldsymbol{D})\nabla\omega)|_b \cdot \boldsymbol{n}. \tag{2.7}$$

Subtracting (2.5) multiplied by ω from (2.7) yields

$$m_s = \frac{1}{1-\omega}\rho(\theta D_m + D_{zz}) \left.\frac{\partial \omega}{\partial z}\right|_b, \tag{2.8}$$

where it has been imposed that the concentration gradient is vertical.

In thermal problems m_s is always null because a prescribed temperature boundary is not a fluid source. However, a prescribed concentration boundary constitutes a source of CO_2 that should be accounted for in fluid mass balance, i.e. flow equation and boundary conditions, as it is a fluid component (Hassanizadeh & Leijnse 1988; Hidalgo *et al.* 2009*b*). Thermal analogies are common in this kind of problems, and they imply neglecting m_s in (2.5). This approach will be termed inconsistent here because the resulting flow and transport balances are not consistent with each other. When m_s is acknowledged, the approach will be termed consistent.

Equation (2.8) might suggest that the CO_2 mass flux across the top boundary is identical to that of the thermal analogies used by, e.g., Riaz *et al.* (2006) or Hassanzadeh *et al.* (2005), except for the factor $(1-\omega)$, which should be close to 1 in practical applications. Actually, there are two other differences. First, the vertical fluid flux at $z = 0$ (2.5) is non-zero. Second, as a consequence, dispersion is activated as a transport mechanism from the outset. Therefore, the effect of this simplification is non-trivial and needs to be assessed through numerical simulations.

2.2. *Dimensionless form*

For analysis purposes, it is convenient to write governing equations in a dimensionless form. Gravity instability, at least for heat transfer between two prescribed temperature plates separated by a distance H, is classically expressed as a function of the Rayleigh number

$$Ra = \frac{u_b H}{\theta D_m}, \tag{2.9}$$

where $u_b = k\Delta\rho g/\mu$, chosen as velocity scale, is the modulus of the buoyancy driving force when $\omega = \omega_s$, and, for CO_2 transport, $\Delta\rho$ is the density contrast between the CO_2-free and the CO_2-saturated brine. However, as mentioned in the introduction, the onset of convection should not be sensitive to H. In fact, the governing equations have been written for a semi-infinite domain, so that there is no natural physical length scale. Therefore, the selection of a length scale is somewhat arbitrary. In diffusive problems it is not uncommon to choose the characteristic length as the one that makes the Rayleigh number equal to 1 (see Rees *et al.* 2008). Doing so, and ensuring also a unit coefficient for time derivatives, leads to the characteristic length and time scales,

$$L_s = \frac{\theta D_m}{u_b}, \quad t_s = \frac{\theta^2 D_m}{u_b^2}. \tag{2.10}$$

It should be noted that t_s depends on porosity squared, instead of simply porosity, which is the usual choice (Tan, Sam & Jamaludin 2003). The difference probably reflects the thermal origin of this kind of formulations and lacks conceptual relevance, but it will be necessary for later comparisons with previous works.

These scales can be generalized to include the effect of dispersion. Therefore, the characteristic length and time scales are chosen as

$$L_s = \frac{\theta D_m + \alpha_L u_b}{u_b}, \quad t_s = \frac{\theta(\theta D_m + \alpha_L u_b)}{u_b^2}. \tag{2.11}$$

Using these scaling factors, the dimensionless form of the flow and transport equations becomes

$$\frac{\partial p'}{\partial t'} + \beta_\omega \frac{\partial \omega}{\partial t'} = -\frac{1}{\rho'}\nabla' \cdot (\rho' \boldsymbol{u}'), \tag{2.12}$$

$$\frac{\partial \omega}{\partial t'} = -\boldsymbol{u}' \cdot \nabla' \omega + \frac{1}{\rho'}\nabla' \cdot (\rho'((1 - b_L)\boldsymbol{I} + b_L \boldsymbol{D}')\nabla' \omega), \tag{2.13}$$

where the prime denotes the dimensionless variables, defined as

$$(x', z') = \frac{1}{L_s}(x, z), \quad t' = \frac{t}{t_s}, \tag{2.14}$$

$$\rho' = \frac{\rho}{\Delta\rho}, \quad p' = \frac{S_p}{\theta} p, \tag{2.15}$$

$$\boldsymbol{u}' = \frac{\boldsymbol{u}}{u_b} = -\frac{\theta}{S_p \Delta\rho g L_s}\nabla' p' - \rho' \hat{\boldsymbol{e}}_z \tag{2.16}$$

and

$$D'_{ij} = r_T \|\boldsymbol{u}'\| \delta ij + (1 - r_T)\frac{u'_i u'_j}{\|\boldsymbol{u}'\|}. \tag{2.17}$$

Dispersion is characterized with the dimensionless numbers of Abarca *et al.* (2007):

$$b_L = \frac{\alpha_L}{L_s} \text{ and } r_T = \frac{\alpha_T}{\alpha_L}. \tag{2.18}$$

Notice that b_L can be viewed as a Rayleigh number defined in terms of dispersion as mass transfer coefficient, instead of D_m, and longitudinal dispersivity α_L as length scale, instead of H. In what follows, Ra as defined in (2.9) is used for classification and comparison purposes, and b_L to describe dispersion.

The resulting boundary conditions are

$$\left.\begin{array}{c} -\rho' \boldsymbol{u}'|_b \cdot \boldsymbol{n} = m'_s \text{ if } z' = 0, \\ \boldsymbol{u}'|_b \cdot \boldsymbol{n} = 0 \text{ for } x' \to \pm\infty, \text{ or } z' \to -\infty, \end{array}\right\} \tag{2.19}$$

for flow and

$$\left.\begin{array}{c} \omega|_b = \omega_s \text{ if } z' = 0, \\ (-\boldsymbol{u}'\omega + ((1 - b_L)\boldsymbol{I} + b_L \boldsymbol{D}')\nabla'\omega)|_b \cdot \boldsymbol{n} = 0 \text{ for } x' \to \pm\infty, \text{ or } z' \to -\infty, \end{array}\right\} \tag{2.20}$$

for transport. Finally, the dimensionless CO_2 mass flux across the top boundary is

$$m'_s = \frac{1}{1 - \omega}\rho'(1 + b_L(u'_z - 1))\frac{\partial \omega}{\partial z'}, \tag{2.21}$$

Parameters maintained constant	Parameters subject to variation
$H = 10$ m	$k = 3.0581 \times 10^{-13}$, 6.1162×10^{-13} m^2
$S_p = 1.02 \times 10^{-8}$ Pa^{-1}	$\alpha_L = 0$–0.5 m
$\mu = 5 \times 10^{-4}$ Pa s	$\alpha_T = 0.1\alpha_L$
$\Delta\rho = 5$ kg m^{-3}	
$\theta = 0.3$	
$D_m = 10^{-9}$ m^2 s^{-1}	

TABLE 1. Parameters used for numerical simulations.

where

$$m'_s = \frac{m_s}{u_b \Delta\rho}. \tag{2.22}$$

3. Numerical analysis

CO_2 dissolution was simulated using the code Transdens (Hidalgo *et al.* 2005). Transdens solves density-dependent flow and transport problems using a finite-element discretization in space and weighted finite differences in time. Reverse time weighting (Saaltink, Carrera & Olivella 2004) is used to minimize mass balance error during time integration. The Darcy velocity is computed using the consistent velocity algorithm by Knabner & Frolkovič (1996). The code has been extensively validated using the usual density-dependent problem benchmarks (Henry, Elder, saltwater bucket and similar problems) and by comparison with other codes (e.g. Hidalgo *et al.* 2005, 2009*b*).

Instabilities in the system were triggered by the propagation of numerical errors. This approach has been subject to some debate. While Schincariol, Schwartz & Mendoza (1994) held that the resulting fingering pattern would not match experimental results, Liu & Dane (1997) showed that it was possible to create physically realistic gravitational instabilities provided that dispersivity values were small. Moreover, Selim & Rees (2007) concluded that the profile of the initial disturbance has little effect on the critical time when the regime becomes unstable given that the disturbance is introduced early enough, which is assured by the highly nonlinear nature of the consistent boundary condition. The ensuing convergence process does introduce disturbances. Therefore, it is assumed that, for the purpose of this work, numerical errors are sufficient to generate instabilities in the system.

Simulations were carried out on a square domain of 10 m $\times$ 10 m (between 17.86 and 2000 in terms of dimensionless distance depending on b_L), which proved to be large enough to warrant that there was no interaction with the lower boundary. The domain was discretized with a mesh of rectangular finite elements of 101 $\times$ 201 nodes. This discretization provides a good balance between numerical precision and computational performance. A sensitivity analysis of discretization showed that results for the onset of convection were little affected when using a finer mesh (a difference smaller than 2 %). The qualitative behaviour of the system was not modified. Parameters (see table 1) were chosen equal to those in Riaz *et al.* (2006) for comparison purposes. Only permeability and dispersivities were subject to change to study their effect on the system behaviour. To facilitate classification and comparison with previous works, the different cases will also be identified by a Rayleigh number as defined in (2.9) using H, the domain thickness, as the characteristic length instead of (2.11).

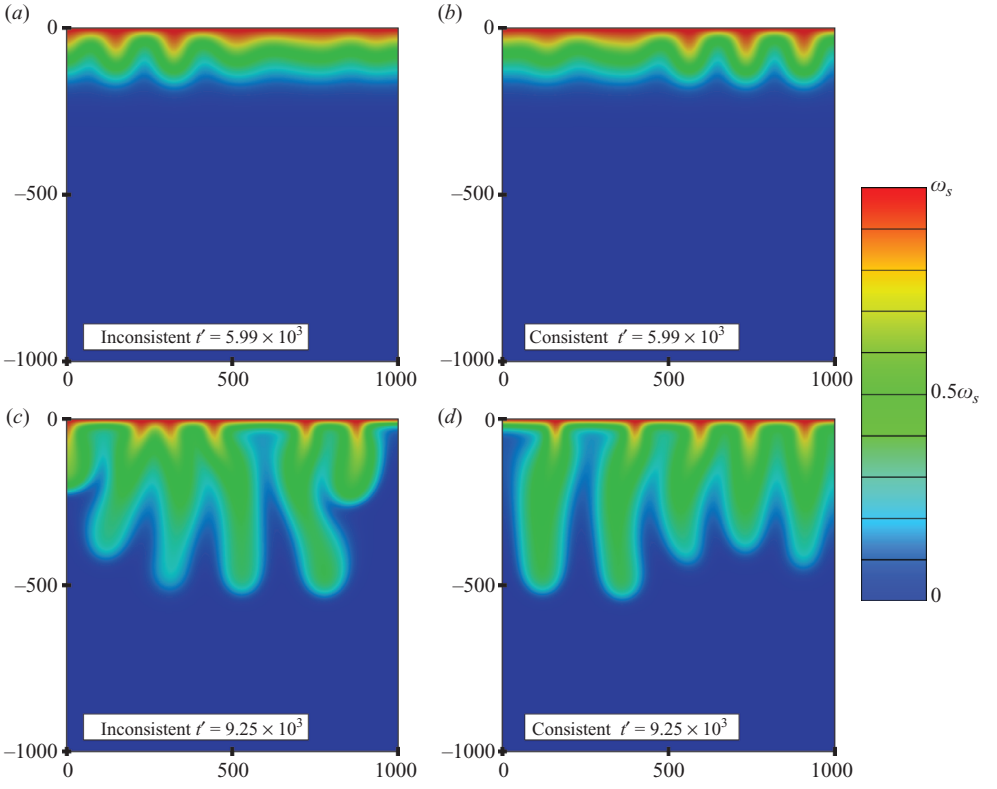

FIGURE 1. CO_2 mass fraction results using the (*a*, *c*) inconsistent and (*b*, *d*) consistent flow and transport boundary conditions for two different times (case $Ra = 1000$, $b_L = 0$, $r_T = 0.1$, $\omega_s = 0.0175$). Colour scale is expressed in terms of fractions of maximum mass fraction ω_s, which equals 0.0175 in this run.

3.1. *Effect of CO_2 flux at the prescribed concentration boundary*

To assess the effect of acknowledging the CO_2 mass influx at the prescribed concentration boundary, the problem was simulated with ω_s equal to 1 and 0.0175. The second one is a realistic value for the CO_2 solubility (Rosenbauer, Koksalan & Palandri 2005). Density contrast was kept identical in both cases by scaling β_ω accordingly. For both values of ω_s, the problem was solved with an inconsistent boundary flow condition ($m'_s = 0$ in (2.19) as in previous works) and with a consistent one (m'_s evaluated at the prescribed concentration boundary).

Results for CO_2 mass fraction are depicted in figure 1, which corresponds to a case in which $Ra = 1000$, $b_L = 0$, $r_T = 0.1$, $\omega_s = 0.0175$. Differences in concentration are moderate for realistic values of ω_s. All solutions display an unstable fingering pattern except for the consistent case with $\omega_s = 1$ (not shown), in which the CO_2 front reaches the lower boundary before fingering has become relevant. The consistent scheme with a realistic value of ω_s leads to thicker fingers that sink slightly faster than the ones in the inconsistent scheme. Differences are due to the slight increase in mass flux caused by the $(1 - \omega)$ term in (2.21) and to the differences in pressure gradient (not shown). Regarding the latter, it should be noticed that in the inconsistent case, as in thermal analogies, fluid density increases at the top boundary without a corresponding

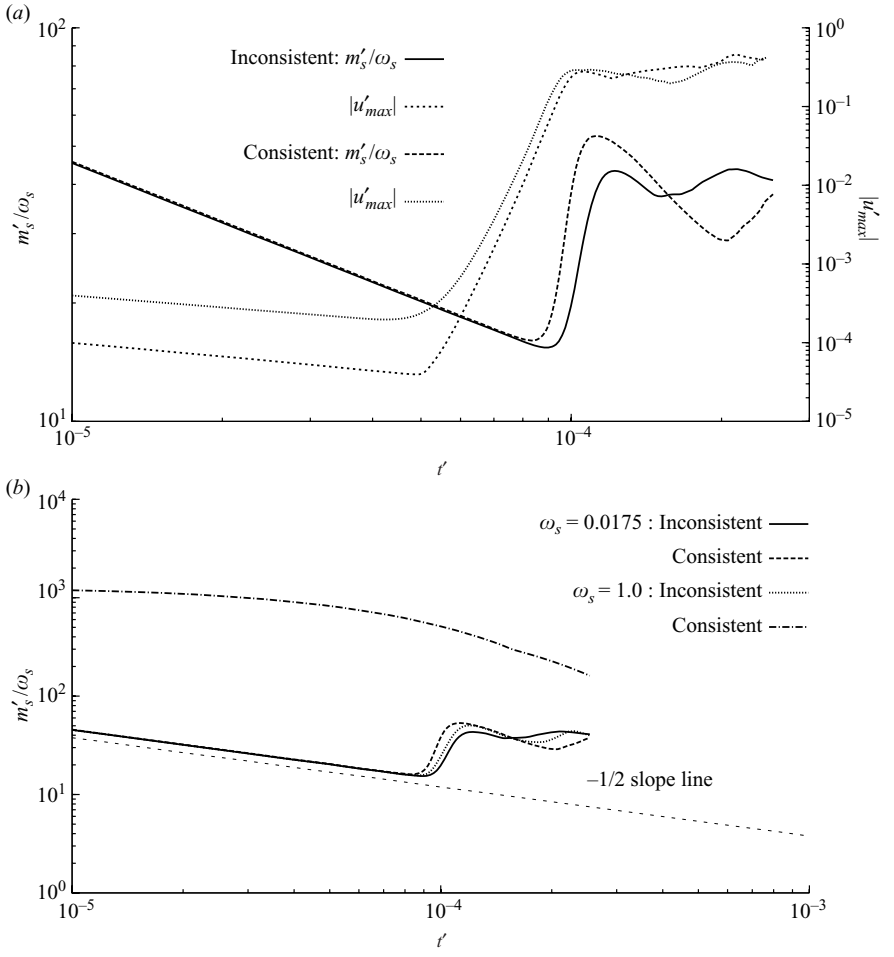

FIGURE 2. (*a*) Evolution of CO_2 mass flux across the top boundary and modulus of maximum velocity evolution for $Ra = 1000$, $b_L = 0.5$, $r_T = 0.1$ and $\omega_s = 0.0175$. (*b*) CO_2 mass flux across the top boundary for the same case and $\omega_s = 0.0175$ and 1.

increase in fluid mass. This can only be compensated by a reduction in pressure. As a result, water flows upwards. This effect is not noticeable in thermal analogies because compressibility effects are neglected and the flux becomes divergence free. The consistent scheme, on the other hand, leads to a pressure increase and fluid to flow downwards. This is important only at the beginning of the simulations. At later times, velocity is dominated by buoyancy and, therefore, independent of the consistency in boundary conditions. This explains why the fingering pattern is not largely affected by boundary conditions.

3.2. *Onset of convection*

The transition from the diffusive to the convective regime can be identified from either the time evolution of the CO_2 mass flux across the top boundary or the modulus of the maximum velocity (figure 2). The diffusive regime is identified by the $-1/2$ slope line in the log-log plot of mass flux versus time. Convection is assumed to be the main transport mechanism when the flux departs from this line. The precise time for onset of convection is defined here as the time when mass flux is minimum (i.e.

when convection is sufficient to compensate the reducing trend of diffusion). This definition will be used to determine the effect of boundary conditions and dispersion on the onset of convection. Notice that this choice leads to slightly larger onset times than the one based on the sharp increase in the modulus of velocity. The mass flux criterion is adopted because the resulting onset time is informative of the time when convective effects become noticeable on CO_2 dissolution rates.

The effect of boundary conditions can be seen in figure 2(*b*). It can be seen that the injection behaviour depends strongly on the value of the prescribed concentration for the consistent case. This is due to the form of the mass flux at this boundary (2.21) which displays a singularity at $\omega = 1$. It causes the difference between the consistent and inconsistent solutions to grow as ω_s tends to 1. The onset time is only slightly affected by the consistency in boundary conditions for reasonable values of ω_s. On the contrary, when $\omega_s = 1$, the mass flux is so dramatically increased that fingering instabilities cannot develop.

A sequence of simulations were performed to assess the effect of dispersion on the onset of convection. The values of b_L range between 0 and 0.995, while r_T is kept constant at 0.1. The b_L range (and accordingly α_L and α_T; see table 1) is consistent with the results obtained by Gelhar, Welty & Rehfeldt (1992) from the analysis of worldwide data on dispersion. They also observed the 1/10 relation between transverse and longitudinal dispersion, which has become a rule of thumb in hydrogeological models. Recently, Bijeljic & Blunt (2007) showed that this relation is adequate when the system is in the convective regime. Only the $\omega_s = 0.0175$ case was simulated, and two different values of Ra were selected (1000 and 2000) by changing k (see table 1).

Results for CO_2 mass flux evolution are shown in figure 3. For the consistent diffusive cases ($b_L = 0$) the convective regime is developed after t' approximately equal to 5600 (some 18 years with the parameters of table 1). In terms of dimensionless time, the onset of convection is independent of the Rayleigh number. The consistent formulation always leads to a reduction in the onset time, which is most significant for moderately large values of b_L. It is interesting to notice that the minimum mass flux is approximately constant and equal to $m'_s = 18\omega_s$. Similarly, it tends to values between $40\omega_s$ and $50\omega_s$ after the onset of convection.

The dependence of the onset time with b_L is best illustrated by figure 4. The onset time decreases linearly with b_L and tends to stabilize for $b_L > 0.96$, which may reflect the smoothing (and stabilization) of the CO_2 front caused by lateral mixing for large dispersion.

Linear regression of the data points for the consistent cases in figure 4 yields

$$t'_{onset} \approx 5619 - 5731 b_L. \tag{3.1}$$

This expression can only be compared with previous results for the case $b_L = 0$. As mentioned in § 2.2, the dimensionless times of Riaz *et al.* (2006) and Tan *et al.* (2003) need to be divided by porosity to be comparable to (3.1). The 5619 dimensionless time of (3.1) for the onset of convection in the absence of dispersion lies between the 487 of Riaz *et al.* (2006) and the 7540 of Tan *et al.* (2003). Differences can be attributed to several factors. First, the model setting is slightly different. Both Riaz *et al.* (2006) and Tan *et al.* (2003) adopted the Boussinesq assumption, which should not make much of a difference, and the here-termed inconsistent boundary condition, which causes a slight overestimation of the onset time. Second, the definition of onset is also slightly different, which may account for a factor of around 2 (recall figure 2). Third, discrepancies may also result from limitations in the numerical scheme. The

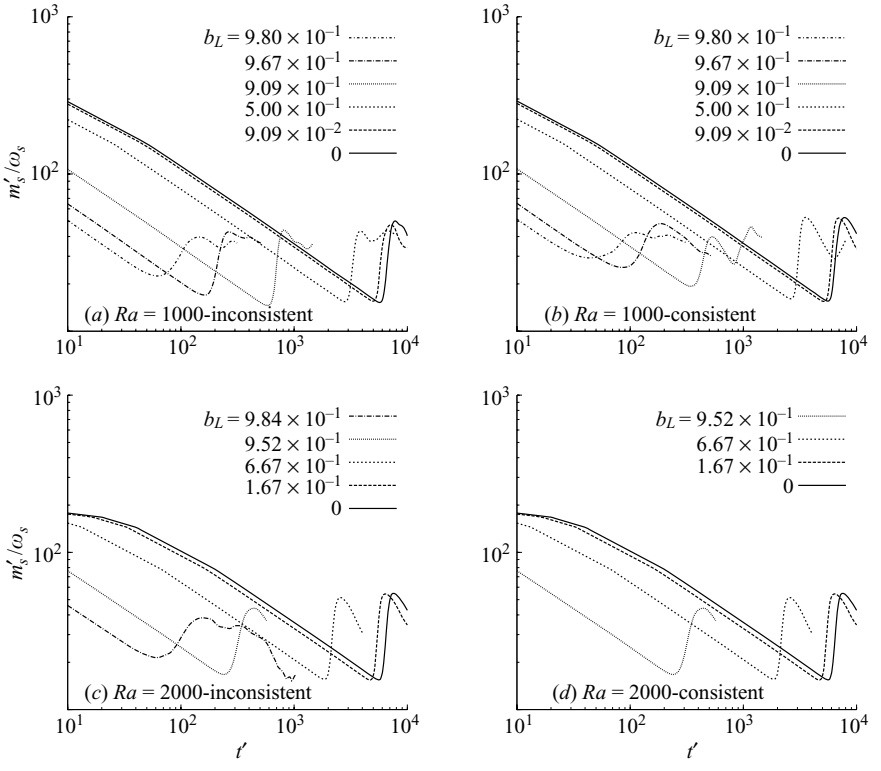

FIGURE 3. CO_2 mass flux across the top boundary for different values of b_L ($r_T = 0.1$, $\omega_s = 0.0175$, $Ra = 1000, 2000$).

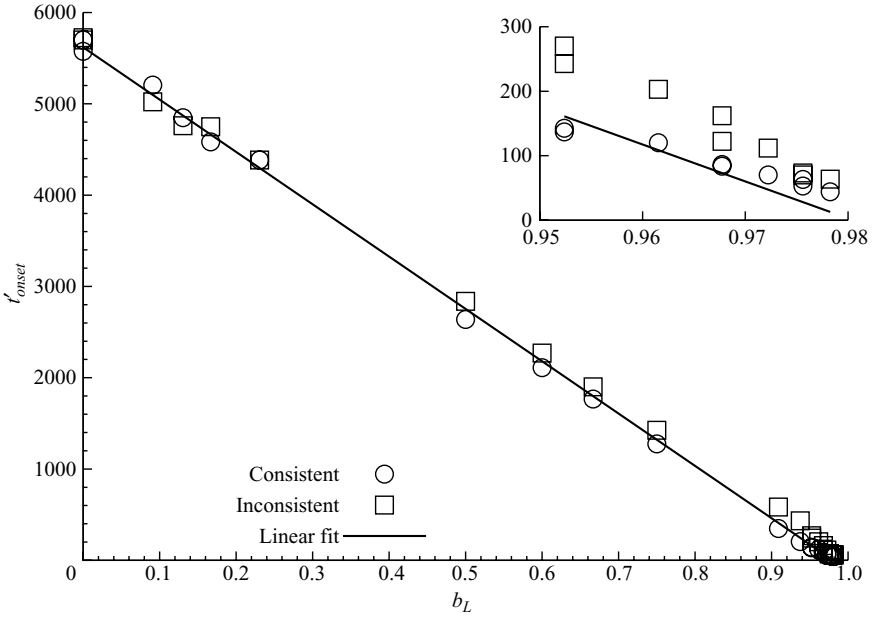

FIGURE 4. Time of the onset of convection for different values of b_L ($r_T = 0.1$, $\omega_s = 0.0175$, $Ra = 1000, 2000$) for the consistent and the inconsistent cases.

selected spatial discretization may be not enough to resolve the smallest wavelength of the problem. Finally, the linear stability analysis behind the 487 dimensionless time tends to underestimate the actual onset time (Riaz *et al.* 2006). In fact, the numerical simulations in figure 14 of Riaz *et al.* (2006), where the position of the most advanced portion of the front as a function of time is plotted, lead to dimensionless onset times between 2000 and 3200, which are comparable to the one of (3.1).

4. Conclusions

The onset of fingering and convective transport can be faster than predicted by previous works. This results mainly from acknowledging CO_2 mass sources in fluid mass balance equations and from including dispersion as a transport mechanism. The compressibility of fluid and medium and the removal of the Boussinesq simplification do not seem to play a critical role. The consistent representation of the CO_2 boundary as a fluid mass source becomes critical only when unrealistically high values of CO_2 solubility are used.

Dispersion, which is present in all real systems, accelerates significantly the time when convection becomes the dominant transport mechanism. In fact, this time decreases linearly with dispersivity, reaching values around 100 times shorter than those of purely diffusive cases. This is important because dispersion can be increased by simply adopting a fluctuating injection regime.

The final version of the paper has greatly benefited from comments by three anonymous referees, one of which motivated the dimensionless formulation adopted. The authors gratefully acknowledge financial support of the Spanish Ministry of Science and Innovation (MICINN) through the PSE-CO_2 project (PSE-120000-2007-6), of the Spanish Government through the Fundación Ciudad de la Energía-CIUDEN and the European Union through project MUSTANG (FP7-ENERGY-2008-1, project number 227286).

REFERENCES

Abarca, E., Carrera, J., Sanchez-Vila, X. & Dentz, M. 2007 Anisotropic dispersive Henry problem. *Adv. Water Resour.* **30** (4), 913–926.

Adams, J. J. & Bachu, S. 2002 Equations of state for basin geofluids: algorithm review and intercomparison for brines. *Geofluids* **2** (4), 257–271.

Bear, J. 1972 *Dynamics of Fluids in Porous Media*. Elsevier.

Bijeljic, B. & Blunt, M. J. 2007 Pore-scale modelling of transverse dispersion in porous media. *Water Resour. Res.* **43** (12), W12S11.

Dentz, M. & Carrera, J. 2003 Effective dispersion in temporally fluctuating flow through a heterogeneous medium. *Phys. Rev.* E **68** (3), 036310.

Ferguson, G. & Woodbury, A. D. 2005 Thermal sustainability of groundwater-source cooling in Winnipeg, Manitoba. *Can. Geotech. J.* **42** (5), 1290–1301.

Gelhar, L. W., Welty, C. & Rehfeldt, K. R. 1992 A critical-review of data on field-scale dispersion in aquifers. *Water Resour. Res.* **28** (7), 1955–1974.

Hassanizadeh, S. M. & Leijnse, T. 1988 On the modelling of brine transport in porous-media. *Water Resour. Res.* **24** (3), 321–330.

Hassanzadeh, H., Pooladi-Darvish, M. & Keith, D. W. 2005 Modelling of convective mixing in CO_2 storage. *J. Can. Petrol. Technol.* **44** (10), 43–51.

Hidalgo, J. J., Carrera, J. & Dentz, M. 2009*a* Steady state heat transport in 3D heterogeneous porous media. *Adv. Water Resour.* **32**, 1206–1212.

Hidalgo, J. J., Carrera, J. & Medina, A. 2009*b* Role of salt sources in density-dependent flow. *Water Resour. Res.* **45**, W05503.

Hidalgo, J. J., Slooten, L. J., Medina, A. & Carrera, J. 2005 A Newton–Raphson based code for seawater intrusion modelling and parameter estimation. In *Groundwater and Saline Intrusion: Selected Papers from the 18th Salt Water Intrusion Meeting, 18th SWIM, Cartagena, 2004* (ed. L. Araguás, E. Custodio & M. Manzano), Hidrogeología y Aguas Subterraneas, vol. 15, pp. 111–120. IGME.

Intergovernmental Panel on Climate Change (IPCC) 2005 *Carbon Dioxide Capture and Storage*. Cambridge University Press.

Johannsen, K. 2003 On the validity of the Boussinesq approximation for the Elder problem. *Comput. Geosci.* **7** (3), 169–182.

Knabner, P. & Frolkovič, P. 1996 Consistent velocity approximation for finite volume or element discretizations of density driven flow in porous media. In *Computational Methods in Subsurface Flow and Transport Problems* (ed. A. A. Aldama, J. Aparicio, C. A. Brebbia, W. G. Gray, I. Herrera & G. F. Pinder), Computational Methods in Water Resources XI, vol. 1, pp. 93–100. Computational Mechanics Publications.

Lackner, K. S., Wendt, C. H., Butt, D. P., Joyce, E. L. & Sharp, D. H. 1995 Carbon-dioxide disposal in carbonate minerals. *Energy* **20** (11), 1153–1170.

Landman, A. & Schotting, R. 2007 Heat and brine transport in porous media: the Oberbeck–Boussinesq approximation revisited. *Transp. Porous Med.* **70** (3), 355–373.

Lindeberg, E. & Bergmo, P. 2003 The long-term fate of CO_2 injected into an aquifer. In *Greenhouse Gas Control Technologies – Sixth International Conference* (ed. J. Gale & Y. Kaya), pp. 489–494. Pergamon.

Liu, H. H. & Dane, J. H. 1997 A numerical study on gravitational instabilities of dense aqueous phase plumes in three-dimensional porous media. *J. Hydrol.* **194** (1–4), 126–142.

Rees, D. A. S., Selim, A. & Ennis-King, J. P. 2008 The instability of unsteady boundary layers in porous media. In *Emerging Topics in Heat and Mass Transfer in Porous Media. From Bioengineering and Microelectronics to Nanotechnology* (ed. P. Vadasz), Theory and Applications of Transport in Porous Media, vol. 22, pp. 85–110. Springer.

Riaz, A., Hesse, M., Tchelepi, H. A. & Orr, F. M. 2006 Onset of convection in a gravitationally unstable diffusive boundary layer in porous media. *J. Fluid Mech.* **548**, 87–111.

Rosenbauer, R. J., Koksalan, T. & Palandri, J. L. 2005 Experimental investigation of CO_2–brine–rock interactions at elevated temperature and pressure: implications for CO_2 sequestration in deep saline aquifers. *Fuel Process. Technol.* **86** (14–15), 1581–1597.

Saaltink, M. W., Carrera, J. & Olivella, S. 2004 Mass balance errors when solving the convective form of the transport equation in transient flow problems. *Water Resour. Res.* **40** (5), W05107.

Schincariol, R. A., Schwartz, F. W. & Mendoza, C. A. 1994 On the generation of instabilities in variable-density flow. *Water Resour. Res.* **30** (4), 913–927.

Selim, A. & Rees, D. A. S. 2007 The stability of a developing thermal front in a porous medium. Part I. Linear theory. *J. Porous Med.* **10** (1), 1–15.

Tan, K.-K., Sam, T. & Jamaludin, H. 2003 The onset of transient convection in bottom heated porous media. *Intl J. Heat Mass Transfer* **46** (15), 2857–2873.

Xu, X. F., Chen, S. Y. & Zhang, D. X. 2006 Convective stability analysis of the long-term storage of carbon dioxide in deep saline aquifers. *Adv. Water Resour.* **29** (3), 397–407.

Yang, C. & Gu, Y. 2006 Accelerated mass transfer of CO_2 in reservoir brine due to density-driven natural convection at high pressures and elevated temperatures. *Indus. Engng Chem. Res.* **45** (8), 2430–2436.